

BNL 51181

Ph. 1689

139
8-29-80

MASTER

**MICROWAVE LONGITUDINAL COUPLING IMPEDANCE
IN ISABELLE VACUUM CHAMBER**

S. GIORDANO AND J. VOTRUBA

March 1980

ACCELERATOR DEPARTMENT

**BROOKHAVEN NATIONAL LABORATORY
ASSOCIATED UNIVERSITIES, INC.**

**UNDER CONTRACT NO. DE-AC02-76CH00016 WITH THE
UNITED STATES DEPARTMENT OF ENERGY**

DISTRIBUTION OF THIS DOCUMENT IS UNLIMITED

DISCLAIMER

This report was prepared as an account of work sponsored by an agency of the United States Government. Neither the United States Government nor any agency Thereof, nor any of their employees, makes any warranty, express or implied, or assumes any legal liability or responsibility for the accuracy, completeness, or usefulness of any information, apparatus, product, or process disclosed, or represents that its use would not infringe privately owned rights. Reference herein to any specific commercial product, process, or service by trade name, trademark, manufacturer, or otherwise does not necessarily constitute or imply its endorsement, recommendation, or favoring by the United States Government or any agency thereof. The views and opinions of authors expressed herein do not necessarily state or reflect those of the United States Government or any agency thereof.

DISCLAIMER

Portions of this document may be illegible in electronic image products. Images are produced from the best available original document.

Master

BNL 51181
UC-28
(Particle Accelerators and
High-Voltage Machines - TID 4500)

MICROWAVE LONGITUDINAL COUPLING IMPEDANCE IN ISABELLE VACUUM CHAMBER

S. GIORDANO AND J. VOTRUBA*

March 1980

*On leave from FZU-CSAV, Prague, Czechoslovakia.

ACCELERATOR DEPARTMENT

BROOKHAVEN NATIONAL LABORATORY
ASSOCIATED UNIVERSITIES, INC.
UPTON, NEW YORK 11973

UNDER CONTRACT NO. DE-AC02-76CH00016 WITH THE
UNITED STATES DEPARTMENT OF ENERGY

DISCLAIMER

This book was prepared as an account of work sponsored by an agency of the United States Government. Neither the United States Government nor any agency thereof, nor any of their employees, makes any warranty, express or implied, or assumes any legal liability or responsibility for the accuracy, completeness, or usefulness of any information, apparatus, product, or process disclosed, or represents that its use would not infringe privately owned rights. Reference herein to any specific commercial product, process, or service by trade name, trademark, manufacturer, or otherwise, does not necessarily constitute or imply its endorsement, recommendation, or favoring by the United States Government or any agency thereof. The views and opinions of authors expressed herein do not necessarily state or reflect those of the United States Government or any agency thereof.

DISTRIBUTION OF THIS DOCUMENT IS UNLIMITED

[Handwritten signature]

DISCLAIMER

This book was prepared as an account of work sponsored by an agency of the United States Government. Neither the United States Government nor any agency thereof, nor any of their employees, makes any warranty, express or implied, or assumes any legal liability or responsibility for the accuracy, completeness, or usefulness of any information, apparatus, product, or process disclosed, or represents that its use would not infringe privately owned rights. Reference herein to any specific commercial product, process, or service by trade name, trademark, manufacturer, or otherwise, does not necessarily constitute or imply its endorsement, recommendation, or favoring by the United States Government or any agency thereof. The views and opinions of authors expressed herein do not necessarily state or reflect those of the United States Government or any agency thereof.

Printed in the United States of America
Available from
National Technical Information Service
U.S. Department of Commerce
5285 Port Royal Road
Springfield, VA 22161
Price: Printed Copy \$4.00; Microfiche \$3.00

SUMMARY

The purpose of this paper is to investigate the modes above the cutoff frequency of the ISABELLE vacuum chamber, and to measure some typical values of the longitudinal coupling impedance. (The investigation was limited to only those modes that have fields in the beam pipe.) Measurements show that the impedance, Z , between 2.6 and 2.8 GHz, can be as high as $10 \times n$ ohms, where n is the ratio of the excitation frequency of the beam divided by the fundamental rotational frequency of the ISABELLE ring. Future work calls for an investigation of the coupling impedance above 2.8 GHz; preliminary work indicates that these impedances Z/n , can be considerably higher than 10 ohms.

1. Definition of Coupling Impedance

The measurement techniques to be developed are based on the fact that the coupling impedance, Z , between the beam and cavities, formed by the vacuum chamber, is identical to the shunt impedance R_s , as defined for linear accelerators, where

$$R_s = \left[\int_0^L E dz \right]^2 / \int_0^L P(z) dz \quad (1)$$

and where E is the actual field as seen by a beam of charged particles travelling through a cavity of length L , and $P(z)$ is the average power loss per unit length along the cavity.

We let $E = E_0 F(z) f(z, t)$, where E_0 is the peak field, $F(z)$ is the spatial field distribution as a function of z , and $f(z, t)$ is dependent on the particle's velocity and position in relation to the phase of the R F field.

If we consider a cavity that has a periodic length L , then the field distribution, $F(z)$, can be decomposed into a Fourier series having spatial harmonics:

$$F(z) = \frac{a_0}{2} + \sum_{k=1}^{\infty} \left(a_k \sin \beta_k z + b_k \cos \beta_k z \right), \quad (2)$$

where the propagation constant $\beta_k = 2\pi k/L$.

We will only consider particles that have a constant velocity v_p ; therefore, z and t are linearly related by the expression $z = v_p t$. The function $f(z, t)$ depends on both the frequency of the cavity, ω_m , and the velocity of the beam. Using the definition that $\omega_m / v_p = \beta_h = 2\pi h / L$, we can now write

$$f(z, t) = \sin\left(\omega_m t + \varphi\right) = \sin\left(\frac{2\pi h z}{L} + \varphi\right), \quad (3)$$

where φ is the phase angle between the beam and cavity voltage.

We can now write Eq. (1) as

$$R_s = \frac{\left\{ \int_0^L \left[\frac{a_0}{2} + \sum_{k=1}^{\infty} \left(a_k \sin \frac{2\pi k}{L} z + b_k \cos \frac{2\pi k}{L} z \right) \right] \sin \left(\frac{2\pi h}{L} z + \varphi \right) dz \right\}^2}{\int_0^L P(z) dz} \quad (4)$$

From the above equation we see that when $k \neq h$, then $R_s \equiv 0$; and when $k = h$, we get $R_s > 0$. It should be emphasized that we are only dealing with synchronous particles, where h is an integer; therefore, the coupling impedance per cavity, of length L , is the same for all cavities.

For nonsynchronous particles, h is not an integer, and, therefore, the phase φ is no longer a constant but varies as a function of z and t . It is still possible to have $R_s > 0$, but the value of R_s will vary as a function of z and t .

2. Perturbation Measurements

We would now like to find the coupling impedance, R_s , by measuring the field distribution along the beam line of a cavity and applying these results to Eq. (4). Figure 1A is a schematic representation of a typical section of the ISABELLE vacuum pipe and pumping stations where the dimensions shown are approximately those of the real machine. We now consider a cavity of length L by placing shorting planes as indicated in Figure 1A. Of interest are the TM_{01m} modes which have an axial electric field distribution E_z , as shown in Figure 1B; it is these fields that contribute to the longitudinal coupling impedance.

The fields are measured by pulling a small metal sphere, of radius $r_0 = 0.0032\text{m}$, along the axis of the cavity. The change in frequency along the cavity is given by

$$\frac{\Delta f(z)}{f} = \frac{\epsilon_0 E_z^2 \pi r_0^3}{W}$$

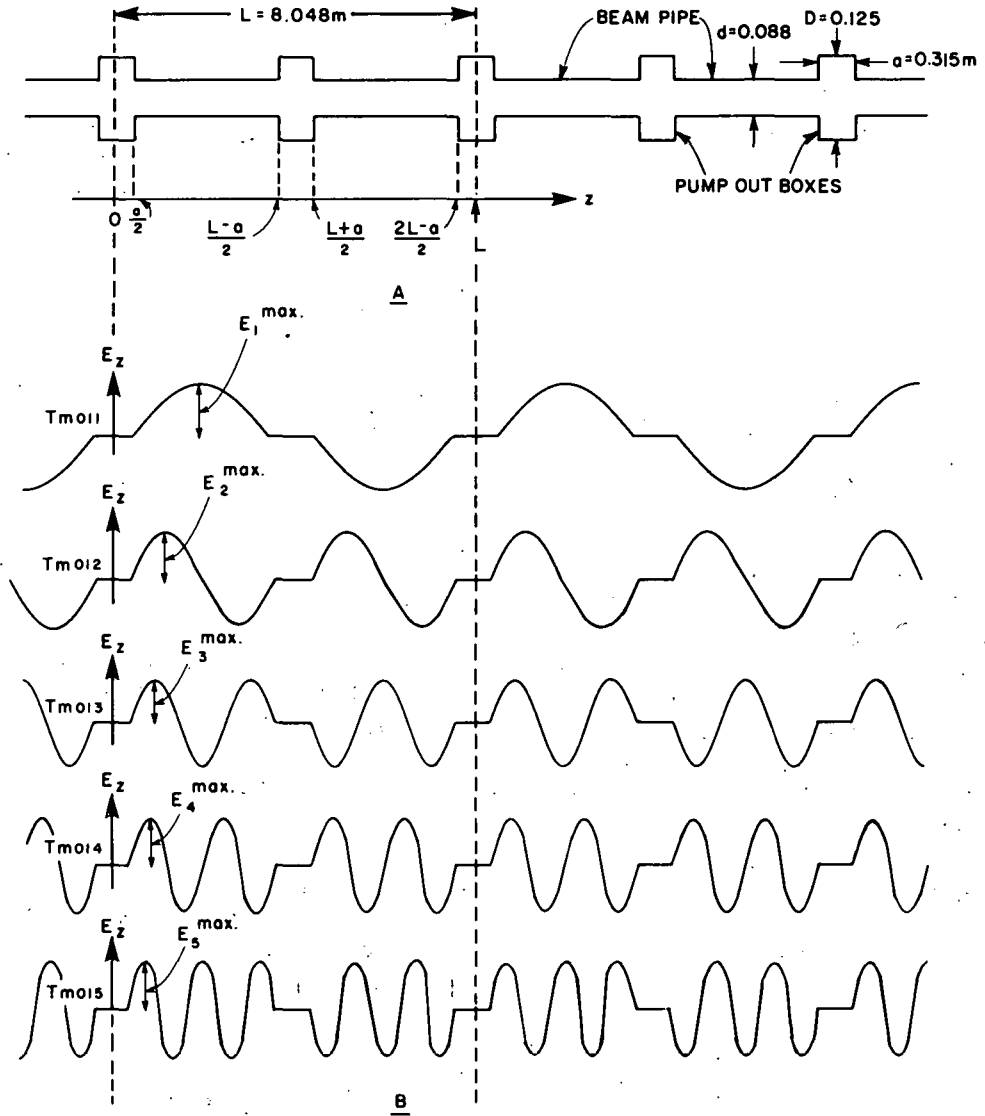


Figure 1A. ISA Vacuum Chamber Model.
 Figure 1B. Some Typical Tm_{0im} Field Distributions.

where E_z is the peak electric field in volts per meter at a point z , $\epsilon_o = 1/(36\pi \times 10^9)$ F/m, W is the stored energy in the cavity in joules, and f is the unperturbed frequency of the cavity. From the above equation we get

$$E_z = \left(\frac{[\Delta f(z)/f] \times W}{\epsilon_o \pi r_o^3} \right)^{\frac{1}{2}} = E_o F(z). \quad (5)$$

By substituting Eqs. (3) and (5) in Eq. (1), and remembering that

$$Q = 2\pi\omega f / \int_0^L P(z) dz,$$

we get

$$R_s = \frac{2Q}{\omega^2 \epsilon_o r_o^3} \left[\int_0^L \sqrt{\Delta f(z)} \left(\sin \frac{2\pi h}{L} z + \varphi \right) dz \right]^2. \quad (6)$$

Equation (6) can now be evaluated for the different TM_{0lm} modes by inserting the measured value of ω_m , Q_m , and $\Delta f_m(z)$. Figure 1B shows some typical measured field distributions which were derived by using the measured values of $\Delta f_m(z)$ and Eq. (5). The actual data can be handled in two different ways: The information for $\Delta f_m(z)$ can be numerically inserted in Eq. (6); or as we were actually able to do, an analytic function can be fitted to the data. It was surprising that a relatively simple function matches the data to a high degree of accuracy. For example, the TM_{0lm} modes, as depicted in Figure 1B, can be described as follows: for the regions 0 to $a/2$, $(L - a)/2$ to $(L + a)/2$, and $(2L - a)/2$ to L , the fields are essentially equal to zero and therefore $\Delta f_m(z) \equiv 0$; and for the regions $a/2$ to $(L - a)/2$, and $(L + a)/2$ to $(2L - a)/2$, the actual field can be described by a simple sine function. We may now rewrite Eq. (6) as

$$R_s = \frac{2Q_m \Delta f_m^{\max}}{\omega_m^2 \epsilon_o r_o^3} \left\{ \int_0^{a/2} 0 \times \sin \left(\frac{2\pi h}{L} z + \varphi \right) dz \right.$$

$$+ \int_{a/2}^{(L-a)/2} \sin \pi \frac{z - a/2}{L/2 - a} \sin \left(\frac{2\pi h}{L} z + \varphi \right) dz$$

$$\left. + \int_{(L-a)/2}^{(L+a)/2} 0 \times \sin \left(\frac{2\pi h}{L} z + \varphi \right) dz \right.$$

$$\begin{aligned}
& + (-1)^m \int_{(L+a)/2}^{(2L-a)/2} \sin m\pi \frac{z - (L+a)/2}{L/2 - a} \sin \left(\frac{2\pi h}{L} z + \varphi \right) dz \\
& + \int_{(2L-a)/2}^L 0 \times \sin \left(\frac{2\pi h}{L} z + \varphi \right) dz \Bigg\}^2, \quad (7)
\end{aligned}$$

where

$$\Delta f_m^{\max} = \frac{\epsilon_0 \pi r_0^3 f_m}{W_m} \times \left(E_m^{\max} \right)^2$$

(see Figure 1B). It is obvious that for our particular cavity, having the fields as shown in Figure 1B, the only spatial harmonics that exist in Eq. (4) are the $a_k \sin 2\pi k z/L$ terms, where $k = 1, 3, 5, \dots$. By comparing Eq. (7) with Eq. (4), it is apparent that for synchronous particles with $\varphi = 0$ we get a maximum R_s for $h = k = (\text{an integer})$. Therefore, Eq. (7) reduces to

$$R_s = \frac{2Q_m \Delta f_m^{\max} L^2}{\omega_m^2 \epsilon_0 r_0^3} \left\{ \frac{\left[1 - 2a/L \right] \left[1 + (-1)^m + h \right]}{m\pi \left[1 - (h/m)^2 (1 - 2a/L)^2 \right]} \sin \frac{\pi h a}{L} \right\}^2. \quad (8)$$

3. Application and Results

Before attempting to apply the above method, it is essential to consider the dispersion curve of the cavity structure. The measured ω vs β diagram is shown in Figure 2 by a solid line, where β is plotted in terms of the spatial harmonic number h . Also included on the diagram are the dispersion curves of the spatial harmonics, as indicated with dashed lines.

The actual measurements were made on a cavity whose length was $L/2$ rather than L . There were two reasons why this was done: The first is that the only model available at that time was $L/2$ long, and the second was that the room in which the measurements were made was too small to accommodate a larger model. The modes actually measured (on this $L/2$ cavity) are shown in Figure 2 as dots. Had the cavity been of length L , other modes would have been measured; these modes are shown by crosses, in Figure 2, and were extrapolated from the data.

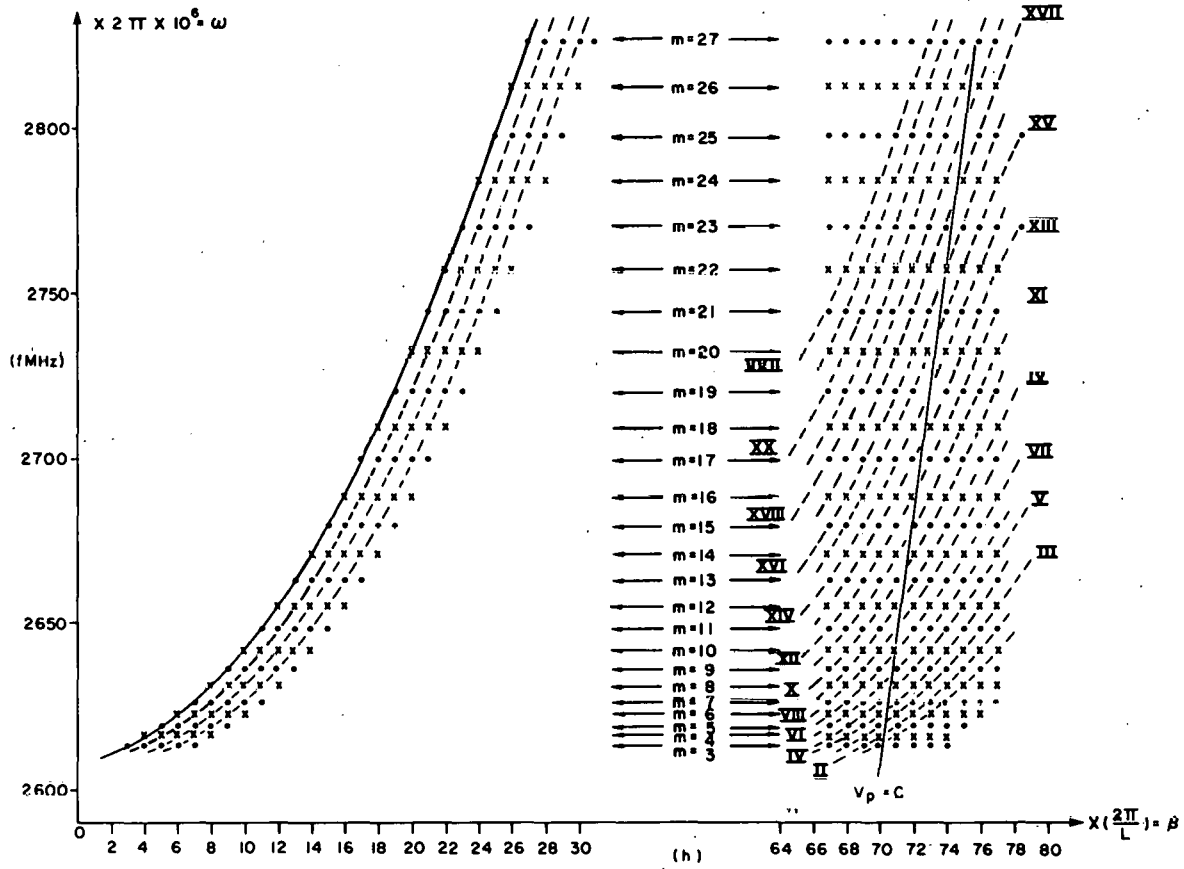


Figure 2. ω vs β Dispersion Curve.

Since we are interested in particles with velocity $v_p = c$, we must now find the spatial harmonics that match this particle velocity, that is $v_p = v_{\phi} = c$. By plotting the line $v_p = c$ in Figure 2, we can immediately determine where this occurs. Using Eq. (8), it is now possible to calculate the shunt impedance as a function of ω_m for the different spatial harmonics that intersect the $v_p = c$ line in Figure 2. The details of these calculations are given in the Appendix, and the results are shown in Figure 3.

4. Conclusions

Of interest to the accelerator builder is the total impedance around the ring as seen by the beam and expressed as a ratio of Z/n , where $Z = R_s \times L_0/L$ (where L_0 is the total length of the structure around the ring, and L , as before, is the length of a single cavity) and $n = f_m/f_0$ (where $f_0 = 78\text{kHz}$, the fundamental rotational frequency of the ISA). For the results given in this paper we used the approximate relation that $Z = 400 \times R_s$. Figure 3 is a plot of the measured Z/n for different modes. It should be noted that some of the modes have a $Z_n \equiv 0$. These modes all have a value of $n + h$ equal to an odd number, and from Eq. (8) we see that the corresponding $R_s \equiv 0$. What this implies, for the particular structure being considered, is that the symmetry of the structure does not allow certain spatial harmonics to exist. The remaining modes shown have relatively narrow resonances where Q_m values are between 4100 and 4600.

If the impedances as measured prove to be troublesome, it would be necessary to change the design of the structure. Some thought has already been given to design changes which would lower the Q_m values and thereby reduce these impedances. Any major change must be carefully considered for its possible impact on other machine design parameters.

Figure 3 does not show all the possible resonances. Measurements were made on a single cavity; and had the structure had more than one cavity many other resonances would have been observed. It is difficult at this time to predict what these other resonances are since the structure will no doubt have stop bands throughout the dispersion curve. A model is now being built to study this problem.

Measurements above 2.8 GHz become difficult due to the mixing of the TM_{01m} modes with other modes. In order to determine R_s above 2.8 GHz another method must be used. In a subsequent paper we will develop a phenomenological method of calculating these impedances. It should be pointed out that preliminary work indicates that R_s above 2.8 GHz will be considerably higher than the numbers given in this paper.

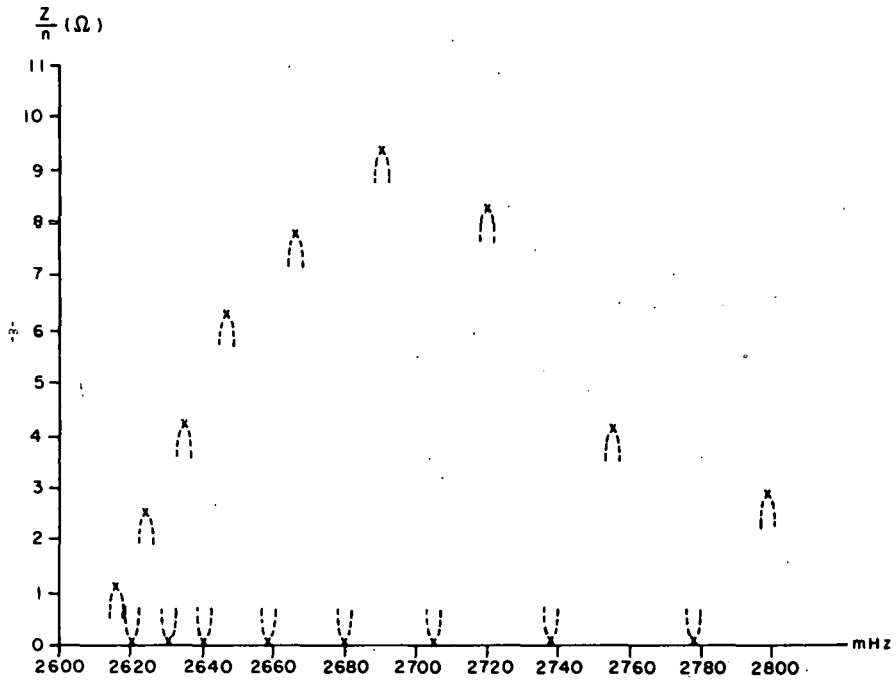


Figure 3. $\frac{Z}{n}$ vs Frequency.

Appendix

To illustrate how Eq. (8) is used to calculate R_s for the different modes, let us consider Figure (4) which is an expanded section of Figure (2). For those curves identified by odd Roman numerals, $R_s \equiv 0$. This results from the fact that for these curves $m + h$ equals an odd number, and when substituted in Eq. (8) we get $R_s \equiv 0$.

For the curves indicated by even Roman numerals, the R_s must be calculated at the point where the curve intersects the line $v_p = c$. At this point, we have the condition that $v_p = v_\phi = c$. There are two cases to be considered:

- (1) The $m = 11$ mode has a spatial harmonic on curve IIX that lies on the line $v_p = c$. It is a simple matter to calculate R_s of this spatial harmonic by substituting in Eq. (8) the values of $m = 11$, $k = 71$, and the measured Q_{11} , ω_{11} , Δf_{11}^{\max} .
- (2) For the curve X, where no spatial mode lies on the line $v_p = c$, R_s must be extrapolated. We first calculate R_s for the points A, B, C, and D as was done in the previous example. Each of these points has its own set of parameters for m , h , Q_m , ω_m and also its own phase velocity $v_\phi = \omega_m/\beta_m = f_m L/h$. The results are plotted in Figure 5, showing R_s vs v_ϕ/c . The condition of interest is where $v_\phi/c = v_p/c = 1$, which corresponds to the interaction of a spatial harmonic wave and particle wave both traveling with a velocity equal to c , and the resulting $R_s = 685 \Omega$. This results in a $Z/n = (400 \times R_s)/n = 8 \Omega$, remembering that $n = f_n/f_0$, as defined in the first paragraph of Section 4.

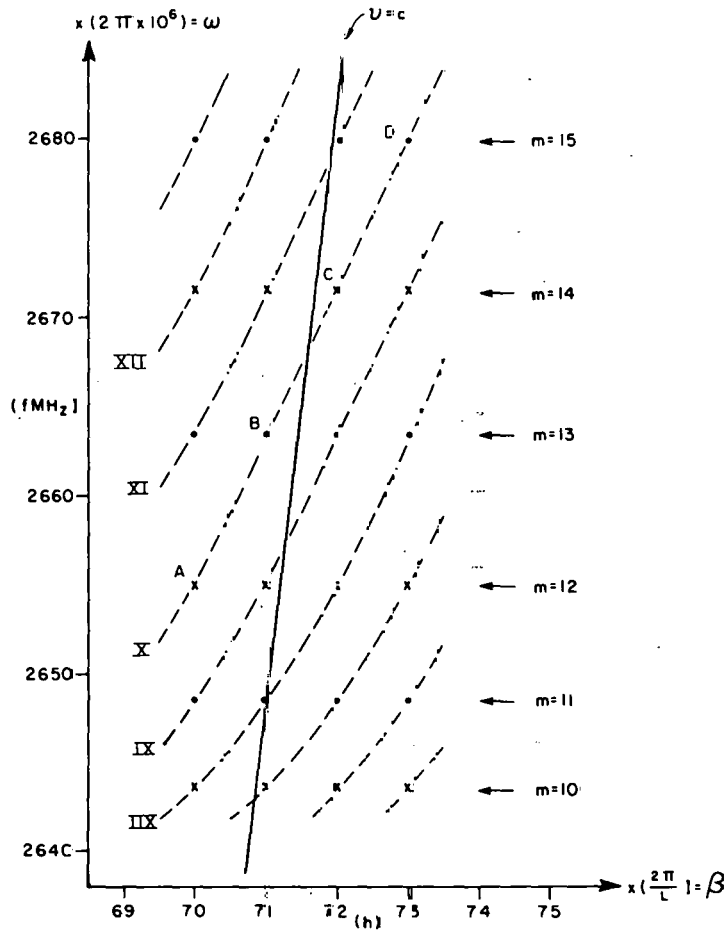


Figure 4. Section of ω vs β Dispersion Curve.

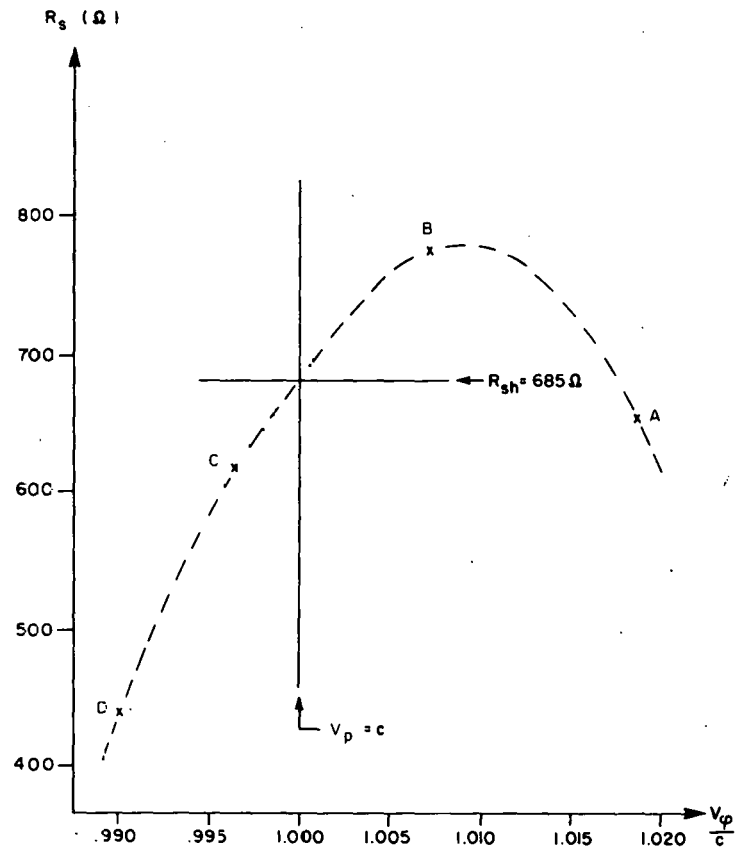


Figure 5. Extrapolation of R_s .